

Bridging the gap between geophysics and geology with Generative Adversarial Networks (GANs)

Suihong Song^{1,2,3}, Tapan Mukerji³, and Jiagen Hou^{1,2}

¹ State Key Laboratory of Petroleum Resources and Prospecting, China University of Petroleum (Beijing), Beijing, 102249, China.

² College of Geoscience, China University of Petroleum (Beijing), Beijing, 102249, China.

³ Stanford University, 367 Panama St, Stanford, CA 94305, USA.

Suihong Song (Email: songsuihong@126.com)

This is a non-peer reviewed preprint submitted to EarthArXiv.

Key Points:

- Generative adversarial networks (GANs) are used to produce geological facies models conditioned to geophysics-interpreted probability maps
- GANs learn geological pattern knowledge and ability of conditioning to the probability maps, well observations, and global features
- The demonstrated GAN framework can be used for similar problems in broad geosciences

Abstract

Inverse mapping from geophysics to geology is a difficult problem due to the inherent uncertainty of geophysical data and the spatially heterogeneous patterns (structure) in geology. We describe GANSim, a type of generative adversarial networks (GANs) that discovers the mapping between remotely-sensed geophysical information and geology with realistic patterns, with a specially designed loss function and an input architecture for geophysics-interpreted probability maps. This GANSim is then used to produce realizations of realistic geological facies models conditioned to the probability maps alone or together with well observations and global features. By evaluation, the generated facies models are realistic, diversified, and consistent with all input conditions. We demonstrate that the GAN learns the implicit geological pattern knowledge from training data and the knowledge of conditioning to inputs from human-defined explicit functions. Given the commonality of probability maps, sparse measurements, and global features, GANSim should be applicable to many problems of geosciences.

Plain Language Summary

Geophysical data (e.g., acoustic wave response data of the subsurface) contains partial information about subsurface geology. Typically, it is first converted into spatial probability maps of geological facies. The probability maps are then used to constrain the spatial distribution of geological facies. The geological facies distribution has certain spatial patterns (structures), related to their depositional environments. When geologists create geological facies maps they need to use two types of knowledge or ability: knowledge of geological facies patterns which are learned by observation of nature, and the ability of letting the maps be consistent with the geophysics-interpreted probability maps and optionally well observations. In this study, we use a deep learning framework, generative adversarial networks (GANs), to build an automatic intelligent generator (a neural network) to grasp these two types of human knowledge. The generator can produce realistic facies distribution models conditioned to input probability maps and optionally well observations and global features. The demonstrated methodology can be used for problems in broad geosciences.

1 Introduction

In geosciences, the objects of interests commonly have complex spatio-temporal patterns, whether in the atmosphere, landforms, oceans, in the Earth's subsurface, or even on the surface of other planets. Apart from sparse point measurements, often one important type of information about these objects is spatially exhaustive remote-sensing geophysical data. These indirect remote-sensing data often have resolution limits and low fidelity, such as satellite-based signals, gravity, magnetic or seismic data. The collected geophysical data are then mapped back into possible target objects that have expected patterns and are consistent with the geophysical data. This inverse mapping process is common in many geoscientific problems like landscape forecast, cloud distribution prediction, and ocean floor forecast. In this paper, we use spatial geological facies distribution as an example of the target objects, along with seismically interpreted probability maps to illustrate the problem of the inverse mapping process and showcase how generative adversarial networks can discover this mapping to generate realistic objects conditioned to geophysical interpretations.

Typically, the geological facies-related geophysical data, such as seismic amplitude or gravity, are first converted into spatially distributed low-resolution (blurry) probability maps of geological facies, based on geophysical inversion and statistical rock physics models (Avseth et al., 2005). Then, geostatistical approaches, such as variogram-based or multiple point statistics (MPS)-based methods, are used to simulate geological facies distribution models conditioned to the geophysics-interpreted probability maps and possibly well observations (see e.g., Remy et al., (2009)), where the spatial patterns of geological facies are introduced in the form of variogram, MPS, etc. One problem for this workflow is the poorly reproduced geological realism in the simulated facies models for complicated sedimentary environments, because the simple statistics (e.g., variogram or MPS) may not be able to represent complete complex spatial patterns of geological facies.

As the most promising generative models in deep learning, generative adversarial networks (GANs; Goodfellow et al., 2014; see also section 2), commonly combined with convolutional neural networks (CNNs; e.g., Krizhevsky et al., 2012), is robust in learning functions to represent complex spatial and temporal patterns and reproducing the learned patterns in newly generated samples. Thus, GANs have been applied for unconditional geological facies modeling with excellent realism (e.g., Song et al., 2020a; Zhang et al., 2019). To produce facies models conditioned to the geophysics-interpreted probability maps, different GAN variants with conditioning effects could be tried. Conditional GAN (CGAN) was proposed by Mirza & Osindero, (2014) and have been used in geosciences, e.g., the cloud vertical structure reconstruction in Leinonen et al., (2019) and CO₂ saturation state prediction in Zhong et al., (2019), but the input conditions are generally of low dimensions such as integer labels. Cycle GAN (Zhu et al., 2017) can translate between high-dimensional domains, e.g., the translation between hydraulic conductivity parameter field and hydraulic head state field in Sun, (2018), yet only one output can be produced for each input condition (i.e., one-to-one mapping), and is not suited for uncertainty quantification in this case where multiple facies models are expected for each probability map. GANSim (Song et al., 2020b) was recently proposed for facies modeling conditioned to sparse well observations and non-spatial global features (e.g., facies proportion), producing realistic and diversified facies models (i.e., one-to-many mapping). It is possible for GANSim to take the high-dimensional probability maps as conditioning data in a similar way to the input well observations condition, and to produce diversified facies models.

In this paper, we design a special loss function in GANSim for the probability maps and build an input pipeline architecture to take in the probability maps. The GANSim is then used for simulation of multiple realistic geological facies models conditioned to the geophysics-interpreted probability maps alone and together with the well observations and one global feature. Through examples, we demonstrate that GANs (or GANSim) can bridge the gap between geophysics and geology, by learning necessary geological pattern knowledge and conditioning rules.

2 Methodology and Data

In GANs, there are two neural networks, a generator (G) and a discriminator (D). Given many observed samples (real) as training data, the generator is trained to generate samples (fake) to resemble the training data, while the discriminator is trained to discriminate the fake samples from real ones. The two networks are alternatively trained until the discriminator cannot discriminate the real samples from the fake ones. Finally, the generator can map a simple probability distribution (e.g., standard Gaussian) into the training data distribution, meaning that the generator learns the underlying pattern knowledge controlling the distribution of training data. For example, if the training data includes many delta facies models, then the generator learns the knowledge of delta distribution patterns.

Traditionally, all layers of GANs are trained concurrently. Karras et al. (2017) proposed progressive growing of GANs, where GANs are trained layer by layer. It allows the underlying pattern knowledge to be learned gradually from coarse to fine scales, and proves to perform better than the traditional GAN training method in training speed, stability, and results quality. We applied the progressive growing of GANs for unconditional facies modeling with excellent results in Song et al., (2020a). Based on that, we proposed GANSim for facies modeling conditioned to sparse well observations and non-spatial global features in Song et al., (2020b). In GANSim, the original unconditional GAN architecture (also called base architecture) is extended to include input pipelines for conditioning data. Figure S1 shows the architectures of generator and discriminator. Table S1 shows the base GAN architecture in detail. An extra condition-based loss function is introduced to combine with the original GAN loss function in GANSim. The original GAN loss, cooperating with the alternative training of generator and discriminator, enforces the learning of the geological facies patterns implicit in the training facies models. The condition-based loss function $L(G)_{con}$ is given by

$$L(G)_{con} = \mathbb{E}_{z \sim p_z, con_{in} \sim p_{con}} Dist(f_{con}[G(z, con_{in})], con_{in}) \quad (1).$$

Here $L(G)_{con}$ represents the inconsistency between input conditioning data con_{in} (i.e., well observations or global features), and the conditioning data computed from the corresponding output generated facies model ($G(z, con_{in})$) through a predefined function f_{con} , that maps the generated facies models into the input conditioning data domain. In the above equation z is the input latent vector, p_z is the distribution of z , p_{con} is the distribution of input condition con_{in} , and $Dist$ is some type of distance function, while \mathbb{E} represents the expectation operator. The condition-based loss function only affects the training of generator G . The minimization of the condition-based loss function enforces the generator to learn the ability of producing facies models that are consistent with the input condition (called conditioning ability).

In this paper, according to the nature of high-dimensionality and the statistical meaning (as a type of probability) of probability maps, we design GANSim to achieve conditioning to the

geophysics-interpreted probability maps of geological facies. The input pipeline for probability maps is designed as follows (Figure 1): at each block of the generator, the probability maps for all facies types except the last one (because the information of the probability map for the last facies type is contained in other probability maps) are first downsampled into the corresponding resolution by averaging; then the downsampled probability maps are transformed into 3D feature cubes of the same resolution, using a 1×1 convolution layer; finally, these 3D feature cubes are concatenated with the corresponding feature cubes in the base generator. The discriminator is the same as that in Figure S1. At the end of each block a facies model of the corresponding resolution is produced through a 1×1 convolution layer in the output pipeline. At the first phase of the training, the downsampled 4×4 -probability maps are taken as input, a 4×4 -facies model is produced, and the first blocks of the generator and discriminator are trained with downsampled 4×4 -training facies models. Then, at the second phase, both 4×4 - and 8×8 -probability maps are taken as inputs, an 8×8 -facies model is produced, and both the first and second blocks of the generator and discriminator are trained with downsampled 8×8 -training facies models. In this way, other blocks of the generator and discriminator are trained gradually one by one at latter phases. When downsampling the training facies models, the most-frequent facies type is kept.

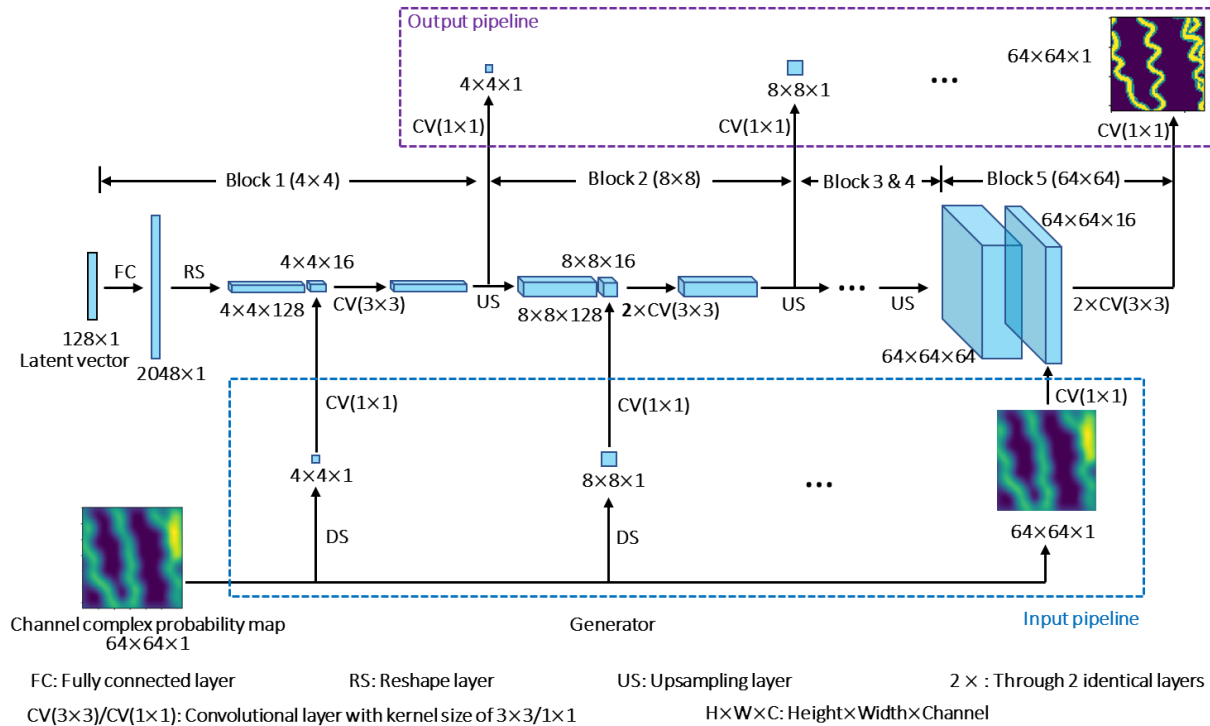


Figure 1. The architecture of the generator for facies modeling conditioned to probability maps. In this figure, the facies models include channel sand (yellow), channel bank (green), and inter channel mud (purple) facies types. The channel sand and channel bank are lumped together as one channel complex facies type when preparing probability maps, so only channel complex probability map is provided into the input pipeline.

By definition, probability is expected to equal frequency (in percentage) of samples. Thus, following the concept of Equation (1), the condition-based loss function for probability maps is defined as:

$$L(G)_p = \mathbb{E}_{z \sim p_z, p \sim p_p} \| f_p(G(z_1, p), G(z_2, p), \dots, G(z_m, p)) - p \|_2 \quad (2)$$

where, z_1, z_2, \dots, z_m are random samples of input latent vector from p_z , p represents input probability maps for all facies types, p_p represents p 's distribution, $Dist$ in Equation (1) is specified as pixel-wise L2 distance, and function f_p calculates the frequency map (in percentage) of each facies type from the m generated facies models, to mimic the real probability map. This loss function expresses the inconsistency between the input conditioning probability maps (p) and the corresponding probability maps calculated from the m generated facies models. m is set to be 8 in this paper. By minimizing this loss function, the input probability maps impose an ensemble-based constraint on multiple generated facies models, allowing each generated facies realization to have enough diversity around the mean model.

In this paper, we initially train GANs only conditioned to the geophysics-interpreted probability maps. However, in many practical applications, in addition to the probability maps, sparse well observations and non-spatial global features are also available, and it is required to further integrate these two types of data to reduce uncertainty of simulated facies models. Therefore, we combine the condition-based loss function of probability maps (Equation (2)) with that of well observations and global features in the original GANSim paper (Song et al., 2020b) together as follows:

$$L(G, D)_{combined} = L(G, D) + \beta_1 L(G)_g + \beta_2 L(G)_w + \beta_3 L(G)_p \quad (3)$$

where, $L(G, D)_{combined}$, $L(G, D)$, $L(G)_g$, $L(G)_w$, $L(G)_p$ are the final combined loss, original GAN loss, and condition-based losses for global features, well observations, and probability maps, and β_1 , β_2 , and β_3 are predefined weights. The input pipelines for the three types of data (i.e., input pipeline in Figure 1 and Figure S1) are applied together. To better tune the weights, we normalize the four losses at the right-hand side of the equation into standard Gaussian distribution, respectively. Finally, a GAN conditioned to all the three types of data is trained.

We use the Wasserstein loss function with gradient penalty (Gulrajani et al., 2017) as the original GAN loss $L(G, D)$. To speed up GAN training, minibatch gradient descent and the Adam optimizer (Kingma & Ba, 2014) are used. The generator and discriminator are alternatively trained with a single minibatch. More details of training are given in Text S1.

To get a visual insight into the relationship among the generated conditional facies models and the real ones (training or test facies models), we use multi-dimensional scaling (MDS) combined with multi-scale sliced Wasserstein distance (MS-SWD) to project their distributions into a 2D space. MS-SWD was proposed by Karras et al., (2017) to evaluate the distance in multi-scale spatial structures between two groups of data. Song et al., (2020a) proposed to combine MS-SWD with MDS to plot the distributions of facies models in 2D space. Text S2 explains MS-SWD-MDS method in more detail. In this paper, MS-SWD is used to calculate pairwise distance between any two of the generated and real facies models, and then each model is projected in the 2D space, using MDS.

The dataset includes 35,640 2D (64×64) synthesized facies models, corresponding global features, 28,5120 sparse well facies data (64×64), and 28,5120 facies probability maps (64×64). The facies models include inter-channel mud, channel sand, and channel bank facies. The channel sand and channel bank are lumped together as one channel complex composite facies in well facies data and probability maps, and only channel complex probability map needs to be

created. We used Gaussian kernel smoothing method to synthesize the channel complex probability map for each facies model. Since in practice probability maps may have diverse resolutions, we defined 8 different Gaussian kernels to produce 8 probability maps (64×64) varying in resolution, for each synthesized facies model. The sizes of these kernels range from 13×13 to 27×27 in odd increments with standard deviations equal to the kernel size in pixels. The global features include mud proportion, channel sinuosity, channel sand width, etc. Figure S3 illustrates some examples of the dataset. Finally, the dataset is randomly split into a training (32,640) and a test (3,000) dataset. The training dataset is used for training GANs, while the test dataset is used for evaluation of the trained generator.

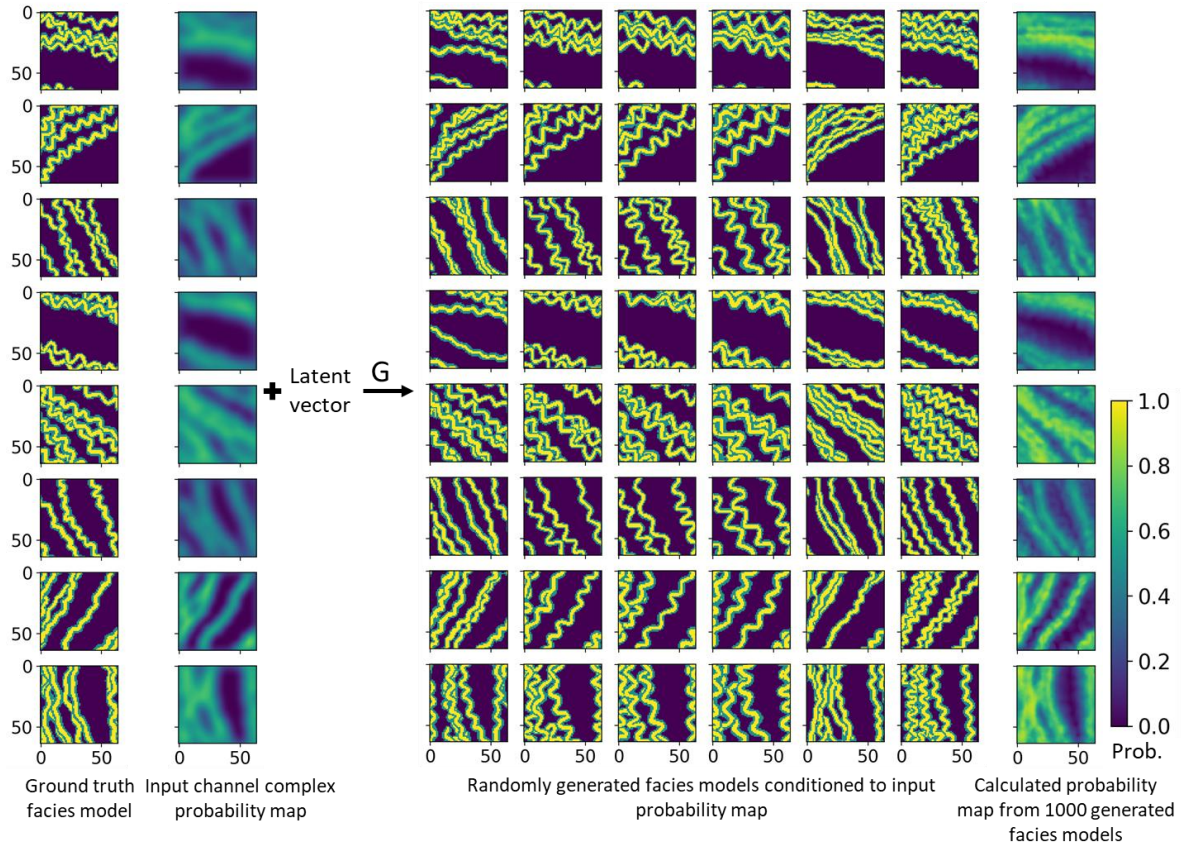
3 Results and discussions

3.1 GAN-based facies modeling conditioned to probability maps

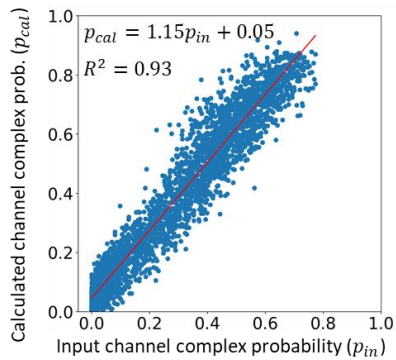
The GAN was trained for 15.5 hours. The inputs of the trained generator include one 64×64 channel complex probability map and one 128-dimension latent vector sampled from the standard Gaussian distribution. Figure 2 (a) shows some generated facies model examples produced by the trained generator, conditioned to random channel complex probability maps in the test dataset. By manual inspection, most of the generated facies models are very realistic, diversified, and consistent with the input probability maps. We calculated channel complex probability map using the function f_p in Equation (2) from 1,000 generated facies models for each probability map condition (see the last column in Figure 2 (a)). The input and calculated probability maps are very similar. We randomly chose 3,000 pixels from 100 pairs of input and calculated probability maps to quantitatively compare their relationship in a cross plot (Figure 2 (b)). The very good correlation between the input and calculated probability values, i.e., very close to $p_{cal} = p_{in}$, proves robust conditioning ability of the trained generator to the input probability map.

The input channel complex probability map controls the large-scale distribution of generated channel complexes, while the input latent vector decides the geometry (e.g., width, sinuosity), facies proportion, and detailed location of the generated channel complexes. In Figure 2 (a), each column of the generated facies models has the same input latent vector. The channel complexes in the third column is narrower than the fourth column, while the channel complexes in the fifth column is straighter than the last column. Compared to other columns, the channel complexes in the first column tend to locate at small-value areas of input probability maps. Figure S4 – S6 show the generated facies models with gradually varying input latent vectors, where the gradual changes of channel complexes can be observed with respect to the geometry and detailed location.

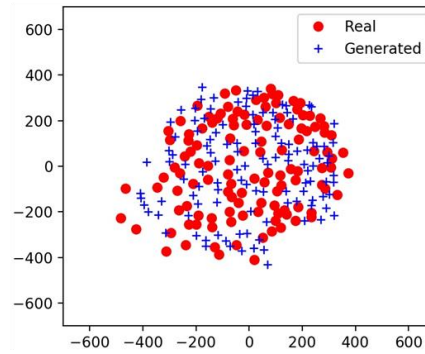
(a) Conditional generated facies models



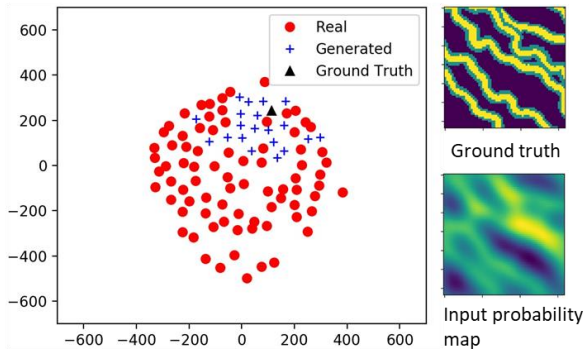
(b) Cross plot between input and calculated prob.



(c) Real vs. generated facies models conditioned to random prob. maps



(d) Real, conditional, and ground truth facies models



(e) Real, conditional, and ground truth facies models

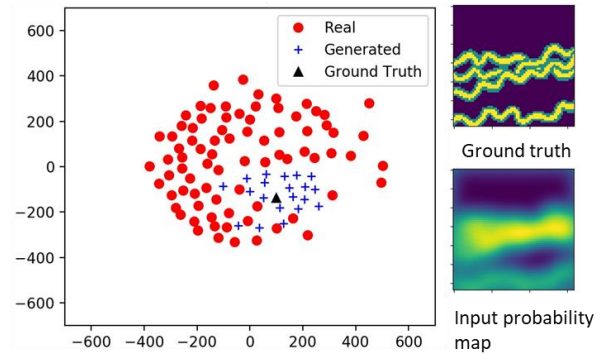


Figure 2. (a) Generated facies models conditioned to input channel complex probability maps from the test dataset and the calculated channel complex probability maps (last column); each column of generated facies models has the same input latent vector. (b) Cross plot between the input and calculated channel complex probability values at 3,000 random pixels from 100 pairs of input and calculated probability maps. (c) Projection of real facies models (from the test dataset) and generated facies models conditioned to random channel complex probability maps in the test dataset in 2D space, based on the MS-SWD-MDS method; each point represents one facies model. (d) - (e) Projection of real, generated conditional, and ground truth facies models in 2D space; the input conditioning probability map is calculated from the ground truth facies model using Gaussian smoothing

Based on MS-SWD-MDS method, Figure 2 (c) projects the distribution of real facies models (from the test dataset) and that of the generated facies models conditioned to various different random probability maps from the test dataset. Their distributions are very close, indicating that the trained generator has learned complete pattern knowledge of geological facies from the training dataset. Figure 2 (d) and (e) show the distribution of real facies models, distribution of generated facies models conditioned to a single probability map, and the ground truth facies model, i.e. the underlying facies model from which the single input probability map was generated by Gaussian smoothing. Compared to Figure 2 (c), the distribution of the generated conditional facies models largely shrinks to cluster closely around the ground truth. This further indicates that the trained generator has learned the conditioning ability to input probability maps.

The MS-SWD-MDS plots also provide insights into the two following questions about information impact: (1) how much information does the geophysics-interpreted probability maps (or geophysical data) carry for the target of forecasting the subsurface geological facies? and (2) how much information is lost from the subsurface geology to the surface-collected low-resolution low-fidelity geophysical data (or the interpreted probability maps)? By comparing Figure 2 (c) to (d) or (e), we see that the introduction of a specific probability map reduces the distribution of the generated facies models from a broad distribution to a narrow one. The reduced distribution space represents the information impact of the input probability map or the underlying geophysical data. The geophysical data or its interpreted probability map is equivalent to the distribution of the generated conditional facies models around the ground truth in Figure 2 (d) and (e), thus the enlarged distribution space from the certain ground truth facies model to the uncertain distribution of the generated conditional facies models represents the information loss by geophysical survey (e.g., seismic survey), with respect to the target of predicting the geological facies.

3.2 GAN-based facies modeling conditioned to probability maps, well data, and mud proportion

We further train a GAN conditioned to the geophysics-interpreted probability map, sparse well observations, and one non-spatial global feature (i.e., mud facies proportion). Weight β_1 , β_2 , and β_3 in Equation (3) are set to be 0.2, 0.25, and 0.2, after trial-and-error numerical experiments. The GAN was trained for 19 hours. Figure 3 (a) shows some facies model examples produced by the trained generator, conditioned to mud proportion value, well facies observations, and channel complex probability map which are all obtained from single real facies model (referred to as the ground truth facies model). Each column of the generated facies models

has the same input latent vector. By visual inspection, the generated facies models are realistic, diversified, and strictly conditioned to the three input conditions.

The channel complex probability map is calculated for each input condition combination (i.e., at each row of Figure 3 (a)). The calculated and the input probability maps are not as similar as in the case of only conditioning to probability maps. This is because the generated facies models are also conditioned to the well observations which are consistent with the input probability maps, thus the generated channel complexes are further pushed towards the high-value areas of the input probability maps. Figure 3 (c) shows the cross plot between the input and calculated probability values at 3,000 random pixels. The trendline ($p_{cal} = 1.32p_{in}$) is steeper than the theoretical one ($p_{cal} = p_{in}$), also because of the above reason. To evaluate the trained generator's conditioning ability to input mud proportion, in Figure 3 (b), we fixed the input well data and probability map as in Figure 3 (a) and gradually increased the input mud proportion value (compared to the ground truth's mud proportion value). It is obvious that, the mud proportion of the generated facies models gradually increases with the input mud proportion value, after conditioning to the input well data and probability map. Figure 3 (d) compares the input and actual (calculated) mud proportion values for 100 randomly generated facies models, further quantitatively proving the trained generator's conditioning ability to the input mud proportion. We also calculated the reproduction accuracy of the input well facies data in generated facies models. The reproduction accuracies for channel complex and mud facies are 99.1% and 97.7%, respectively, proving the trained generator's robust conditioning ability to input well observations. Similar to the previous case of only conditioning to probability maps, the input latent vector controls the geometry of generated channel complexes. The location of channel complexes is influenced by both the input well data and the input latent vector, after being consistent with the input probability map.

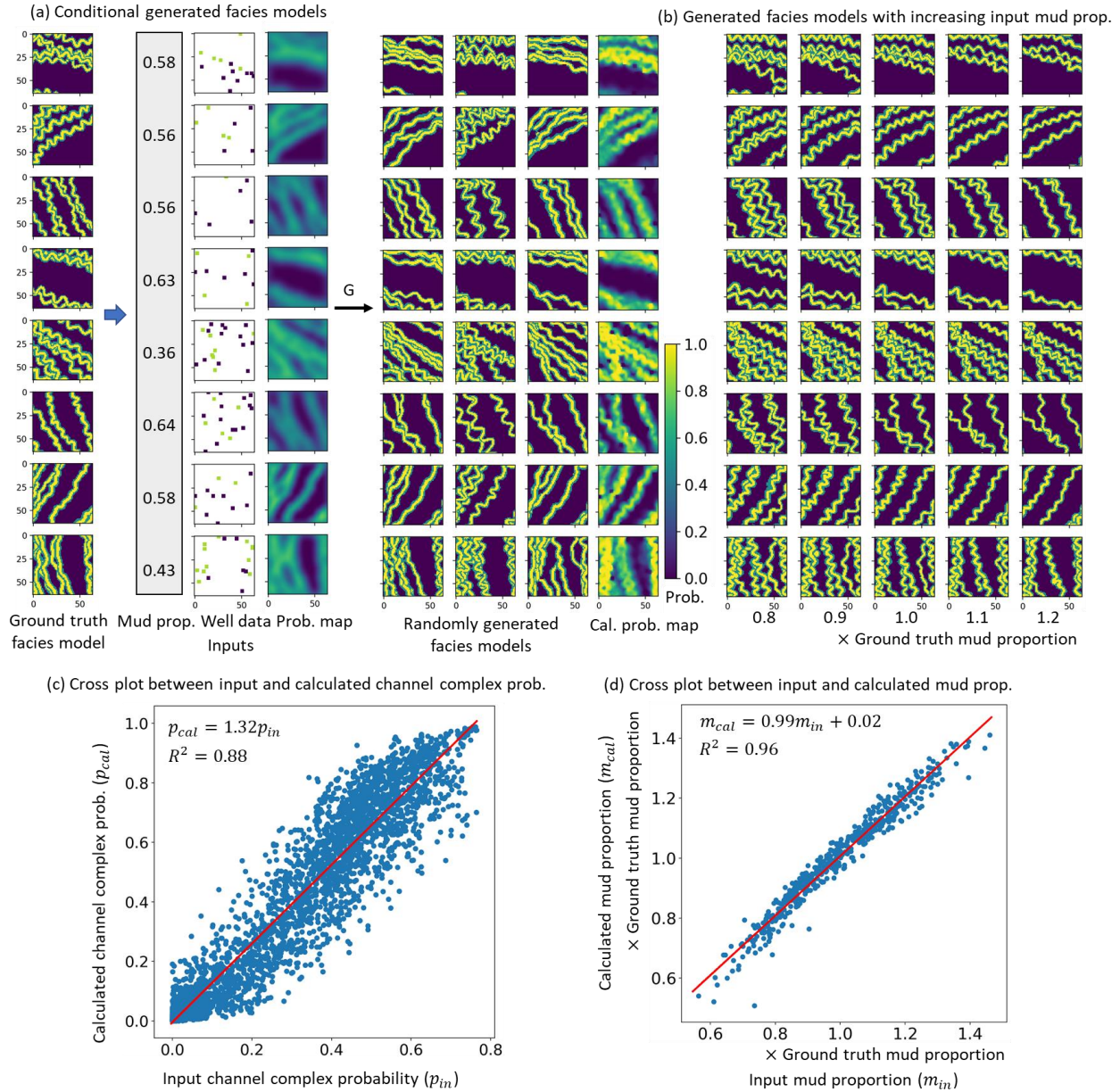


Figure 3. (a) Generated facies models conditioned to the input mud proportion, well facies data, and channel complex probability map, and calculated channel complex probability map (last column); (b) Generated facies models with increasing input mud proportion value and fixed input well data, probability map, and latent vector. (c) Cross plot between the input and calculated channel complex probability values at 3,000 random pixels from 100 pairs of input and calculated probability maps. (d) Cross plot between the input and actual (calculated) mud proportion values for 100 randomly generated facies models.

3.3 Insights into GAN-based knowledge learning in geosciences

In geosciences, the objects (x) that we study (e.g., geological facies) commonly involve certain intrinsic spatial or temporal patterns (pat), and the obtained remote-sensing geophysical information (y) about these objects is generally incomplete, in terms of resolution, measurement

density, or fidelity. Predicting the underlying geological objects from the obtained incomplete geophysical information is actually a conditional probability problem: producing $p(x|(pat, y))$. The spatio-temporal patterns are difficult to be completely represented with general statistics or explicit analytical functions.

GANs are robust in learning pattern knowledge involved in training data and reproducing the learned patterns in newly generated samples, i.e., producing $p(x|pat)$ where $x|pat$ represents the target object. To directly produce $p(x|(pat, y))$ for any given y , the generator needs to further learn the mapping rules from y and $p(x|pat)$ to $p(x|(pat, y))$ (i.e., the conditioning ability). There are different sources for this learned knowledge. The pattern knowledge is learned from training data through the original GAN loss function. The mapping rule knowledge can be learned from human-based knowledge (e.g., the predefined function f_p in Equation (2) of this paper), paired dataset (e.g., in conditional GAN), or cyclicity between domains (e.g., in cycle GAN) all through the minimization of loss functions. As Reichstein et al., (2019) concluded, domain knowledge can be learned through either constraints in loss function or neural network architecture. Here we have used both aspects – design of appropriate loss functions, as well as design of network architecture – to enable GANs to learn spatial patterns along with data conditioning.

4 Conclusions

Mapping from uncertain geophysical data into geology can be framed in terms of conditional probabilities involving the inherent patterns of geology. We use generative adversarial networks (GANSim) to produce realizations from the conditional distribution of realistic geological facies models conditioned to geophysics-interpreted probability maps (and possibly well observations and non-spatial global features), thus bridging the gap between geophysics and geology. Given the commonality of the three types of data (i.e., spatially-distributed physics-interpreted probability maps, sparse point measurements, and non-spatial global features) and the problem of predicting target objects with spatial patterns in geosciences, GANSim, as demonstrated in this study, has great implications for similar problems in other geosciences, such as remote sensing retrieval, climate forecast, environment forecast, and landscape prediction, that involve spatial patterns and low resolution remote-sensing information.

Acknowledgments

This work was supported by the National Science and Technology Major Projects of China (No. 2016ZX05014002). We acknowledge the sponsors of the Stanford Center for Earth Resources Forecasting (SCERF) and support from Prof. Steve Graham, the Dean of the Stanford School of Earth, Energy and Environmental Sciences. Some of the computing for this project was performed on the Sherlock cluster at Stanford University. We would like to thank Stanford University and the Stanford Research Computing Center for providing computational resources and support that contributed to these research results. Codes, data, and some results of this work are available at [Github.com/SuihongSong/GeoModeling_Conditional-to-Probability-maps-plus](https://github.com/SuihongSong/GeoModeling_Conditional-to-Probability-maps-plus) (<https://doi.org/10.5281/zenodo.3977852>).

References

- Avseth, P., Mukerji, T., & Mavko, G. (2005). *Quantitative seismic interpretation: Applying rock physics tools to reduce interpretation risk*. Cambridge University Press, <https://doi.org/10.1017/CBO9780511600074>
- Goodfellow, I., Pouget-Abadie, J., Mirza, M., Xu, B., Warde-Farley, D., Ozair, S., et al. (2014). Generative Adversarial Networks. In *Advances in Neural Information Processing Systems 27*. <https://doi.org/10.1001/jamainternmed.2016.8245>
- Gulrajani, I., Ahmed, F., Arjovsky, M., Dumoulin, V., & Courville, A. (2017). Improved Training of Wasserstein GANs. *ArXiv E-Prints*, arXiv:1704.00028.
- Karras, T., Aila, T., Laine, S., & Lehtinen, J. (2017). Progressive Growing of GANs for Improved Quality, Stability, and Variation. *ArXiv E-Prints*, arXiv:1710.10196.
- Kingma, D., & Ba, J. (2014). Adam: a method for stochastic optimization. *ArXiv Preprint ArXiv:1412.6980*. <https://doi.org/10.1109/ICCE.2017.7889386>
- Krizhevsky, A., Sutskever, I., & Hinton, G. E. ImageNet Classification with Deep Convolutional Neural Networks, *Advances in Neural Information Processing Systems 25* § (2012). <https://doi.org/10.1117/12.2176558>
- Leinonen, J., Guillaume, A., & Yuan, T. (2019). Reconstruction of Cloud Vertical Structure With a Generative Adversarial Network. *Geophysical Research Letters*. <https://doi.org/10.1029/2019GL082532>
- Mirza, M., & Osindero, S. (2014). Conditional Generative Adversarial Nets. *ArXiv E-Prints*, arXiv:1411.1784.
- Reichstein, M., Camps-Valls, G., Stevens, B., Jung, M., Denzler, J., Carvalhais, N., & Prabhat. (2019). Deep learning and process understanding for data-driven Earth system science. *Nature*. <https://doi.org/10.1038/s41586-019-0912-1>
- Remy, N., Boucher, A., & Wu, J. (2009). *Applied Geostatistics with SGeMS: A user's guide*. *Applied Geostatistics with SGeMS: A User's Guide*. <https://doi.org/10.1017/CBO9781139150019>
- Song, S., Mukerji, T., & Hou, J. (2020a). Geological Facies Modeling Based on Progressive Growing of Generative Adversarial Networks (GANs). *EarthArXiv*. <https://doi.org/10.31223/osf.io/ycufs>
- Song, S., Mukerji, T., & Hou, J. (2020b). GANSim: Conditional Facies Simulation Using an Improved Progressive Growing of Generative Adversarial Networks (GANs). *EarthArXiv*. <https://doi.org/10.31223/osf.io/fm24b>
- Sun, A. Y. (2018). Discovering State-Parameter Mappings in Subsurface Models Using Generative Adversarial Networks. *Geophysical Research Letters*. <https://doi.org/10.1029/2018GL080404>
- Zhang, T. F., Tilke, P., Dupont, E., Zhu, L. C., Liang, L., & Bailey, W. (2019). Generating geologically realistic 3D reservoir facies models using deep learning of sedimentary architecture with generative adversarial networks. *Petroleum Science*. <https://doi.org/10.1007/s12182-019-0328-4>
- Zhong, Z., Sun, A. Y., & Jeong, H. (2019). Predicting CO₂ Plume Migration in Heterogeneous Formations Using Conditional Deep Convolutional Generative Adversarial Network. *Water Resources Research*. <https://doi.org/10.1029/2018wr024592>
- Zhu, J. Y., Park, T., Isola, P., & Efros, A. A. (2017). Unpaired Image-to-Image Translation Using Cycle-Consistent Adversarial Networks. In *Proceedings of the IEEE International Conference on Computer Vision*. <https://doi.org/10.1109/ICCV.2017.244>

Supporting Information for

Bridging the gap between geophysics and geology with Generative Adversarial Networks (GANs)

Suihong Song^{1,2,3}, Tapan Mukerji³, and Jiagen Hou^{1,2}

¹ State Key Laboratory of Petroleum Resources and Prospecting, China University of Petroleum (Beijing), Beijing, 102249, China.

² College of Geoscience, China University of Petroleum (Beijing), Beijing, 102249, China.

³ Stanford University, 367 Panama St, Stanford, CA 94305, USA.

Corresponding author: Jiagen Hou (jghou63@hotmail.com)

Contents of this file

Figures S1 to S6

Table S1

Text S1 and S2

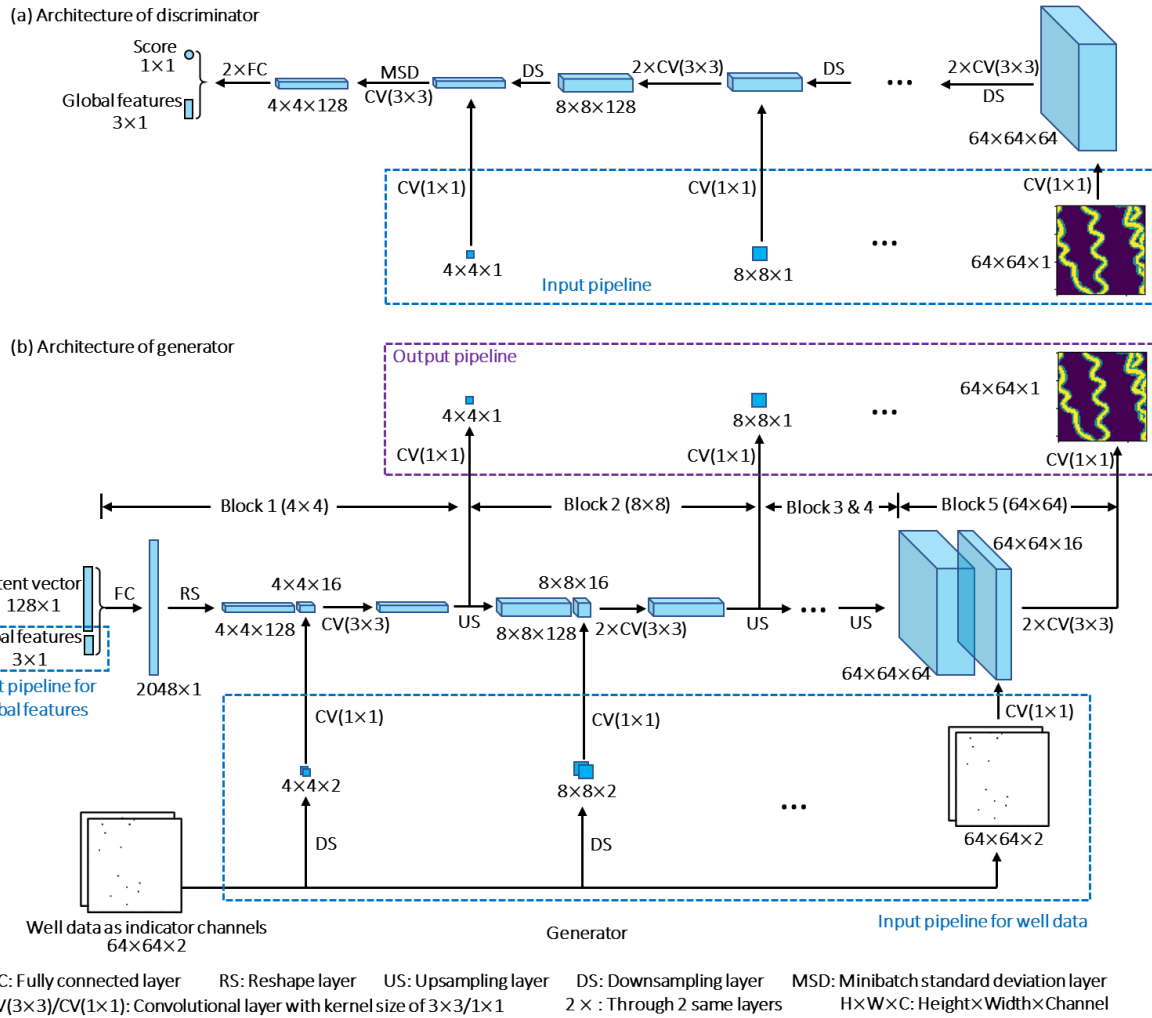


Figure S1. The architectures of the generator and discriminator used in the original GANSim (Song et al., 2020b) for facies modeling conditioned to well observations and non-spatial global features.

Table S1. The detailed architectures of the base generator and discriminator used in this study

Generator					Discriminator				
Block	Layer	Activation	Output shape	No. of trainable parameters	Block	Discriminator	Activation	Input shape	No. of trainable parameters
	Latent vector	-	128×1	-		Input image	-	$64 \times 64 \times 1$	-
Block 1 (4×4)	Fully connected	LReLU	2048×1	262k	Block 5 (64×64)	Convolutional 1×1	LReLU	$64 \times 64 \times 1$	128
	Reshape	-	$4 \times 4 \times 128$	-		Convolutional 3×3	LReLU	$64 \times 64 \times 64$	37k
	Convolutional 3×3	LReLU	$4 \times 4 \times 128$	148k	Convolutional 3×3	LReLU	$64 \times 64 \times 64$	74k	
Block 2 (8×8)	Upsampling	-	$8 \times 8 \times 128$	-	Downsampling	-	$64 \times 64 \times 128$	-	
	Convolutional 3×3	LReLU	$8 \times 8 \times 128$	148k	Convolutional 3×3	LReLU	$32 \times 32 \times 128$	148k	
	Convolutional 3×3	LReLU	$8 \times 8 \times 128$	148k	Block 4 (32×32)	Convolutional 3×3	LReLU	$32 \times 32 \times 128$	148k
Block 3 (16×16)	Upsampling	-	$16 \times 16 \times 128$	-	Downsampling	-	$32 \times 32 \times 128$	-	
	Convolutional 3×3	LReLU	$16 \times 16 \times 128$	148k	Convolutional 3×3	LReLU	$16 \times 16 \times 128$	148k	
	Convolutional 3×3	LReLU	$16 \times 16 \times 128$	148k	Block 3 (16×16)	Convolutional 3×3	LReLU	$16 \times 16 \times 128$	148k
Block 4 (32×32)	Upsampling	-	$32 \times 32 \times 128$	-	Downsampling	-	$16 \times 16 \times 128$	-	
	Convolutional 3×3	LReLU	$32 \times 32 \times 128$	148k	Convolutional 3×3	LReLU	$8 \times 8 \times 128$	148k	
	Convolutional 3×3	LReLU	$32 \times 32 \times 128$	148k	Block 2 (8×8)	Convolutional 3×3	LReLU	$8 \times 8 \times 128$	148k
Block 5 (64×64)	Upsampling	-	$64 \times 64 \times 128$	-	Downsampling	-	$8 \times 8 \times 128$	-	
	Convolutional 3×3	LReLU	$64 \times 64 \times 64$	74k	Minibatch std. dev.	-	$4 \times 4 \times 128$	-	
	Convolutional 3×3	LReLU	$64 \times 64 \times 64$	37k	Block 1 (4×4)	Convolutional 3×3	LReLU	$4 \times 4 \times 129$	149k
	Convolutional 1×1	Linear	$64 \times 64 \times 1$	65	Fully connected	LReLU	2048×1	262k	
Total trainable parameters				1.41M	Fully connected	Linear	128×1	129	
					Total trainable parameters				1.41M

**Convolutional 3×3 / Convolutional 1×1: Convolutional layer with kernel size of 3×3 / 1×1.

Text S1:

Some details of GAN training

Since the Wasserstein loss (Gulrajani et al., 2017) can stabilize the training process of GANs, we alternate between training the generator and training the discriminator both with single minibatch. The Adam optimizer (Kingma & Ba, 2014) with default parameters is used in this work. Each minibatch includes 32 facies models. The training schedule includes 20,000 training iterations for phase 1 (4×4), 40,000 training iterations for each phase from phase 2 (8×8) to phase 4 (32×32), and unlimited number of iterations for phase 5 (64×64) until stopping criteria are achieved. The stopping criteria include manual inspection of the realism, diversity, and the conditioning effects of generated facies models. In this work, 2 GPUs (NVIDIA Tesla V100-PCIE-32GB), 10 CPUs, and 80G RAM are used in parallel for training.

Text S2:

Multi-scale sliced Wasserstein distance (MS-SWD) combined with multi-dimensional scaling (MDS)

MS-SWD is proposed by Karras et al. (2017) to evaluate the distance in multi-scale spatial structures between two groups of data. Here we show the calculation steps of MS-SWD with an example of two groups of facies models (64×64 , 2D). As Figure S4 shows, each group contains M facies models. First, the Laplacian pyramid representations (Burt & Adelson, 1987) of each facies model in both groups is calculated from resolution of 64×64 to 16×16 . The Laplacian pyramid representations reveal the structures of the original facies models at different scales. Second, multiple (n) small patches ($p \times p$ pixels) are randomly extracted from the Laplacian pyramid representation of each facies model at each level, to obtain $M * n$ patches from each group of facies models at each level. Third, these patches are normalized with respect to the mean and the standard deviation of each patch. Finally, the sliced Wasserstein distance (SWD), an efficient approximation to the Wasserstein distance (Rabin et al., 2012), between the patches from each group at each level is calculated. MS-SWD over different levels can be averaged as single value to represent the distance between two distributions.

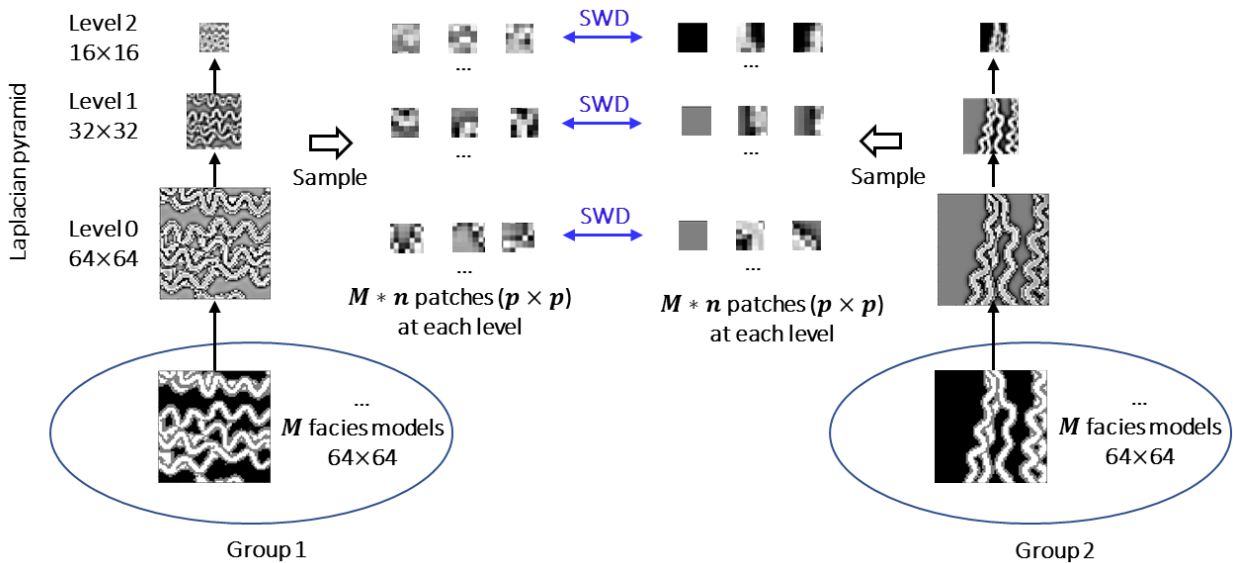


Figure S2. A schematic illustration of how MS-SWD is calculated with an example of two groups of 2D facies models.

MDS is commonly used to project high-dimensional data into 2D or 3D space to visualize their relationship, based on certain type of distance between each pair of the data. MS-SWD is originally used to calculate the distance between two large groups of data. Song et al., (2020a) proposed to combine MS-SWD with MDS (MS-SWD-MDS) to project the two groups of data into 2D space. In the method, each large group is divided into many small groups, and the MS-SWD is calculated for each pair of the small groups inside the two large groups. Then, all small groups are projected into 2D space using MDS, based on the calculated MS-SWD (average of MS-SWD) among these small groups. Each point in MDS represents one small group of data.

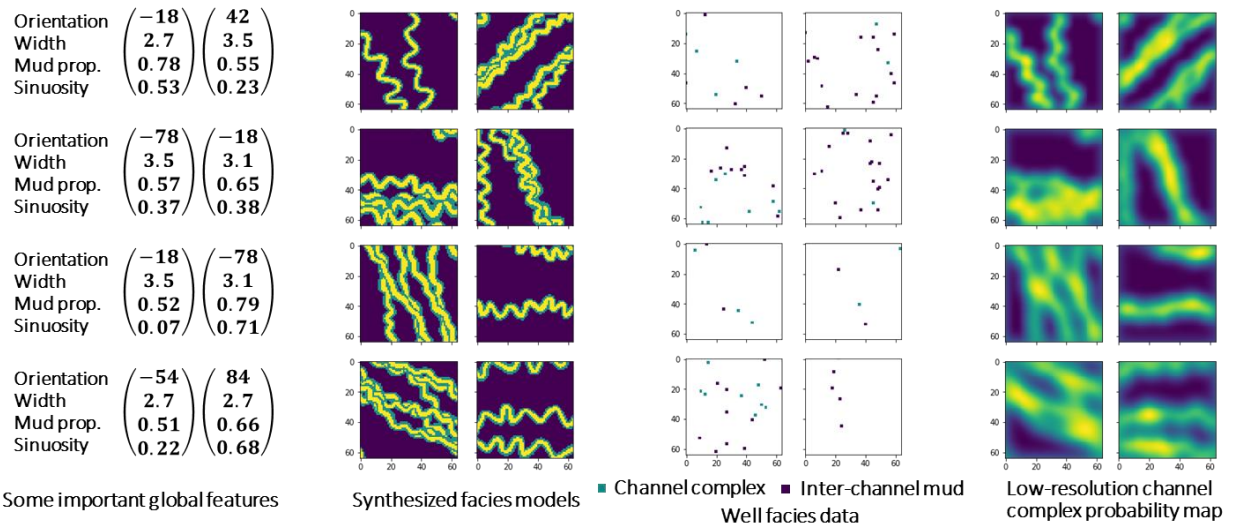


Figure S3. Random examples of the facies models and corresponding global features, sparse well facies data, and probability maps.

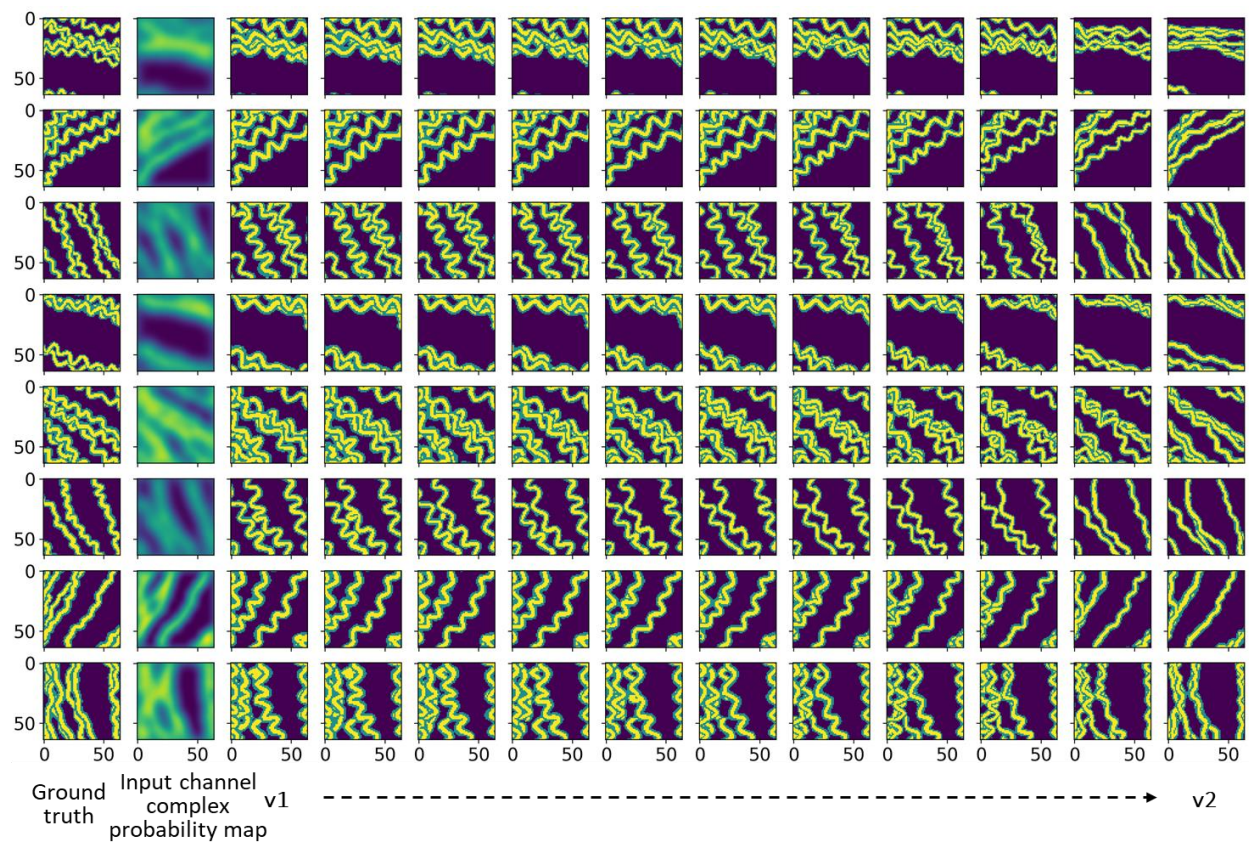


Figure S4. The generated facies models conditioned to input channel complex probability maps. Each column of the generated facies models has the same input latent vector. The latent vectors vary in the gradual deformation manner (see Hu, (2000)) from random vector v_1 to another random vector v_2 .

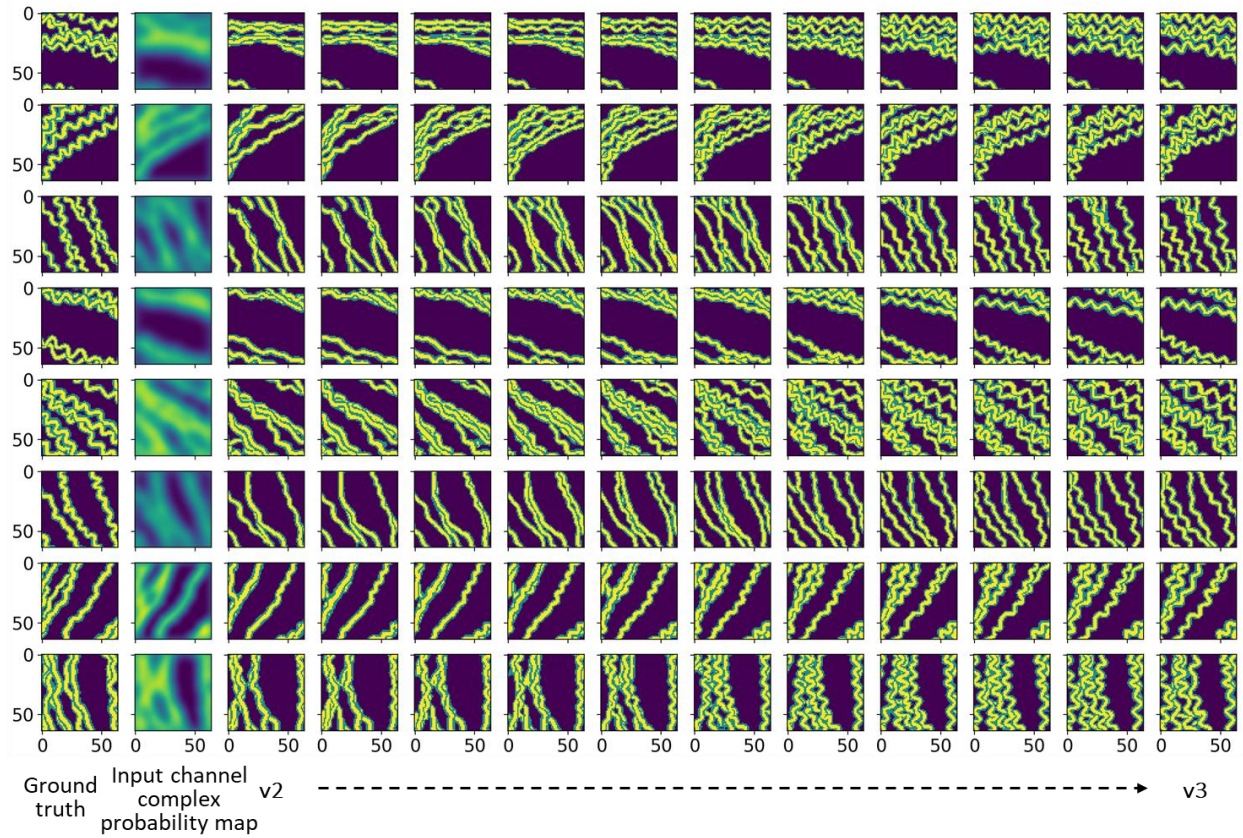


Figure S5. The generated facies models conditioned to input channel complex probability maps. Each column of the generated facies models has the same input latent vector. The latent vectors vary in the gradual deformation manner (see Hu, (2000)) from vector v_2 in (Figure S4) to another random vector v_3 .

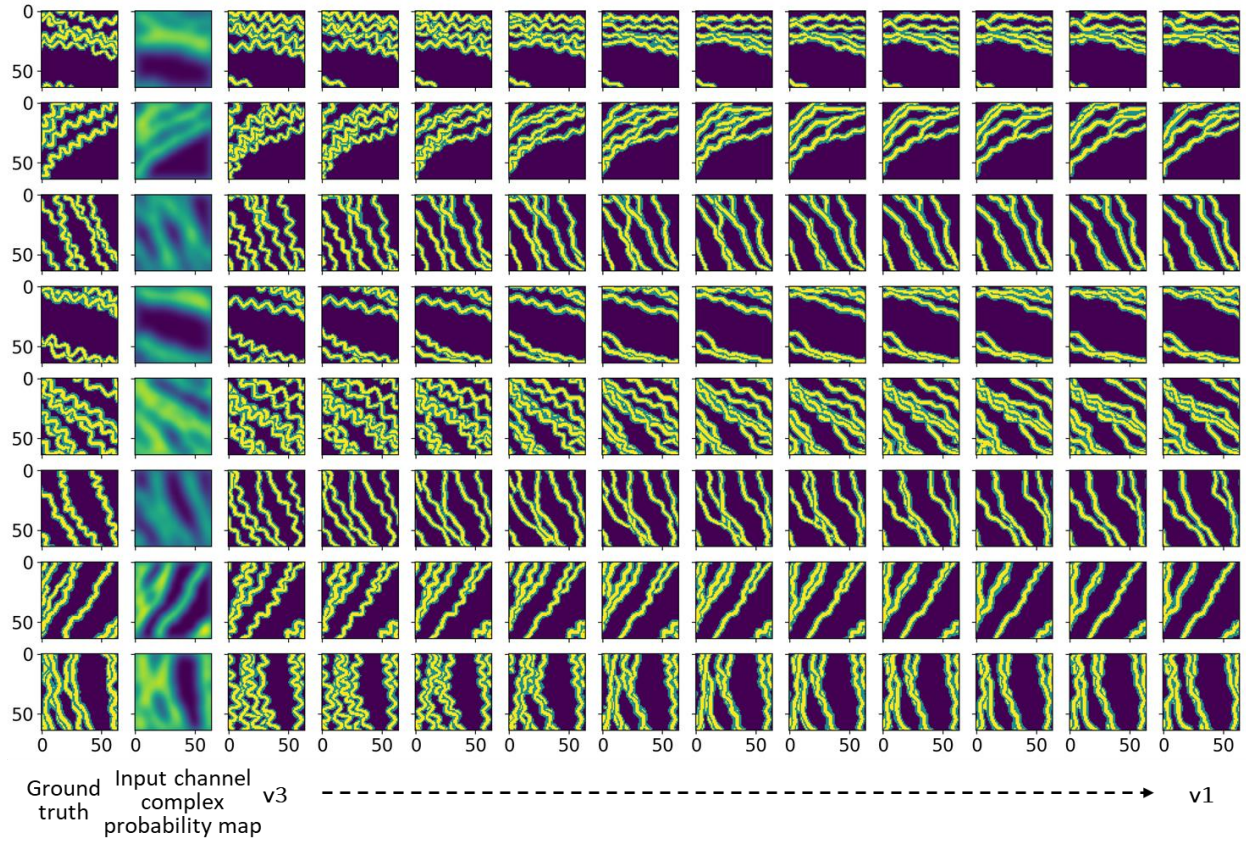


Figure S6. The generated facies models conditioned to input channel complex probability maps. Each column of the generated facies models has the same input latent vector. The latent vectors vary in the gradual deformation manner (see Hu, (2000)) from random vector v_3 (in Figure S5) to another random vector v_1 (in Figure S4).

References

- Burt, P. J., & Adelson, E. H. (1987). Readings in Computer Vision: Issues, Problems, Principles, and Paradigms. In M. A. Fischler & O. Firschein (Eds.) (pp. 671–679). San Francisco, CA, USA: Morgan Kaufmann Publishers Inc. Retrieved from <http://dl.acm.org/citation.cfm?id=33517.33571>
- Gulrajani, I., Ahmed, F., Arjovsky, M., Dumoulin, V., & Courville, A. (2017). Improved Training of Wasserstein GANs. *ArXiv E-Prints*, arXiv:1704.00028.
- Hu, L. Y. (2000). Gradual deformation and iterative calibration of Gaussian-related stochastic models. *Mathematical Geology*. <https://doi.org/10.1023/A:1007506918588>
- Karras, T., Aila, T., Laine, S., & Lehtinen, J. (2017). Progressive Growing of GANs for Improved Quality, Stability, and Variation. *ArXiv E-Prints*, arXiv:1710.10196.
- Kingma, D., & Ba, J. (2014). Adam: a method for stochastic optimization. *ArXiv Preprint ArXiv:1412.6980*. <https://doi.org/10.1109/ICCE.2017.7889386>
- Rabin, J., Peyré, G., Delon, J., & Bernot, M. (2012). Wasserstein Barycenter and Its Application to Texture Mixing. In A. M. Bruckstein, B. M. ter Haar Romeny, A. M. Bronstein, & M. M. Bronstein (Eds.), *Scale Space and Variational Methods in Computer Vision* (pp. 435–446). Berlin, Heidelberg: Springer Berlin Heidelberg.
- Song, S., Mukerji, T., & Hou, J. (2020a). Geological Facies Modeling Based on Progressive Growing of Generative Adversarial Networks (GANs). *EarthArXiv*. <https://doi.org/10.31223/osf.io/ycufs>
- Song, S., Mukerji, T., & Hou, J. (2020b). GANSim: Conditional Facies Simulation Using an Improved Progressive Growing of Generative Adversarial Networks (GANs). *EarthArXiv*. <https://doi.org/10.31223/osf.io/fm24b>